

Supplementary material for

Intraseasonal to interannual variability of zooplankton biomass and standing stock inferred from ADCP backscatter in the eastern Arabian Sea

R. K. Sahu^{1,2}, D. Shankar^{1,2,*}, P. Amol^{1,3}, S. G. Aparna^{1,2}, D. V. Desai^{1,2}

¹*CSIR National Institute of Oceanography, Dona Paula, Goa-403004, India.*

*Corresponding author (Email: shankar@nio.res.in)

²*Academy of Scientific and Innovative Research (AcSIR), Ghaziabad, 201002, Uttar Pradesh, India*

³*CSIR-NIO, Regional Centre, Visakhapatnam, 530017, Andhra Pradesh, India*

- 1 The supplementary material consists of a detailed comparison with biomass climatology
2 from (Aparna et al., 2022) (henceforth, A22). A brief introductory section about com-
3 ponents of seasonal cycle and variabilities followed by overview of analysis tools used to
4 identify the former are presented.

5 **S1 Comparison with biomass and ZSS climatology
6 of A22**

- 7 It is observed that D215 is shallower at all locations and as a result a lower biomass and
8 ZSS as seen in the climatology of the present study (Fig. S1). The difference in D215 is
9 prominent off Goa; while in the previous climatology the D215 is deeper and lies along
10 D23, in the present climatological data the D215 is shallower and lies ~20–40 m above
11 the D23 during January to April. A relatively lower biomass is present above z215 year
12 round which reflects in overall lower ZSS of Goa and Mumbai. In the present data, the
13 ZSS maximum off Mumbai occurs in March instead of February (A22), due to a lower
14 ZSS value. The second maximum occurs in August and is less pronounced in recent data
15 (Fig. S1 d1, d2). There is dramatic decrease in the minimum off Mumbai that occurs in
16 October and ZSS increases rapidly afterwards till February, and the minor peak seen in
17 A22 is not observed off Mumbai. Off Kollam, higher biomass occurs from May to June in
18 A22, and from May to June and September to November in the present study, with a ZSS
19 minimum in August. The higher ZSS on either side to this minimum is less pronounced
20 in A22. This difference in ZSS with regard to A22 is clearly seen in the correlation of
21 A22 and present ZSS climatology, which is 0.60 off Kollam, 0.94 off Mumbai, and 0.98 off
22 Goa. In the present study, chl-a biomass peaks across all locations in August, and a minor
23 peak off Mumbai. Off Kollam, a zooplankton-phytoplankton relationship discrepancy is
24 consistent with A22 findings. The climatological values of chl-a and ZSS is depicted in
25 TableTable S1.

26 **S2 Variability and analysis techniques**

27 **S2.1 Interannual, annual, and intra-annual variability**

28 The mean biomass, standard deviation at 40 m and 104 m, and the surface-to-deep
29 biomass difference is presented in [Tabletable](#) S2. Biomass time series exhibit variability
30 across distinct temporal bands, from daily to multi-year scales. The most fundamental is
31 diel vertical migration, with higher biomass at depth during the day and near the surface
32 at night.

33 On longer timescales, interannual variability arises due to changes in monsoon-driven
34 upwelling. This variability appears in two forms: (1) quasi-periodic changes with periods
35 > 400 days, evident in the wavelet power (\sim 600–800 days) off Mumbai, Goa, and Kollam
36 (Fig. 9), and (2) aperiodic deviations from the typical seasonal cycle (Fig. 5).

37 Annual variability (300–400 days) reflects seasonal shifts (Fig.S2, left), while intra-
38 annual variability (100–250 days) captures transitions between seasons. At the NEAS,
39 both summer and winter monsoons drive chl-*a* blooms, but asymmetries in wind forcing
40 lead to a stronger semi-annual cycle (Jensen, 1993; Schott and McCreary, 2001) (Fig. S2,
41 right; Section 3.2). Intraseasonal variability (5–90 days) stems from short-term environ-
42 mental changes (Fig. 11), with biomass bursts lasting from a few days to several weeks,
43 often coinciding with mesoscale current activity (Amol et al., 2014; Chaudhuri et al.,
44 2020) (Section. 5).

45 In annual-band plots, contours of biomass peaks often tilt upward, indicating upward
46 phase propagation. While less pronounced than in the annual WICC cycle (Amol et al.,
47 2014; Chaudhuri et al., 2020, 2021), this tilt suggests physical–biological coupling. It
48 occurs intermittently across all variability bands and results in phase differences between
49 surface and deep biomass time series. In-phase signals at both depths yield higher or
50 lower column-integrated biomass (e.g., Oct–Nov 2019; Fig.S3), while phase offsets (e.g.,
51 Mar–May 2019) lead to subdued values. Such phase lags between depths or moorings
52 can be further analyzed via wavelet coherence (Section. S2.2.1).

53 **S2.2 Wavelet analysis and filtering methods**

54 It is essential to first understand Fourier analysis before we discuss wavelet analysis.
55 Fourier analysis decomposes a time series into a sum of sine and cosine functions. The
56 resulting power spectrum reveals peaks that correspond to the dominant periods or fre-
57 quencies within the signal. This approach is particularly effective for analyzing signals
58 with known periodic components, such as annual (360 days) and semi-annual (180 days)
59 cycles with fixed periodicity.

60 Fourier analysis can obscure the non-stationary signals of a time series and can mis-
61 represent the power at a given period. However, real world cases includes non-stationary
62 signals and therefore wavelet analysis is needed to deal with time series data (Torrence
63 and Compo, 1998; Maraun and Kurths, 2004) as it provides a representation of time
64 series in time-frequency domain. It employs wavelets, a localized wave-like functions that
65 can be customized by varying wavelet’s scale and position along the time series to iden-
66 tify periodic (stationary) and irregular (non-stationary) patterns and their strength with
67 time. This analysis is routinely used in time series data in the field of oceanography and
68 geophysics, biomedical engineering and signal processing etc.

69 **S2.2.1 Wavelet analysis**

70 Wavelet analysis has a crucial role to identify the periods of variability whether they
71 are continuous round the year as in the annual cycle or discrete bursts that shows up in
72 spectra within the intraseasonal band. Biomass time series at 40 and 104 m is chosen and
73 decomposed to time (abscissa) vs frequency (ordinate) domain (Fig. 6). The horizontal
74 lines extending from the ordinate indicate specific periods. The color intensity along each
75 line in the wavelet spectrum reflects the strength and persistence of the corresponding
76 periodic signal over time. Two additional features should be noted: 1) the cone of
77 influence (CoI), which delineates regions where edge effects caused by the finite length of
78 the time series may distort the spectral power; and 2) contours of statistical significance,
79 which highlight regions of the spectrum where the detected features are unlikely to be
80 due to random variability. A feature must be within the CoI and statistically significant
81 to make correct interpretation on the observed variability in the time series. For example,
82 at the annual scale (365 days) off Mumbai (Fig. 6), intensity of wavelet spectra is high,
83 it lies well within CoI, and is statistically significant. The semi-annual cycle is seen along
84 with bursts in intraseasonal time scales.

85 Wavelet coherence builds upon the continuous wavelet transform, allowing for the
86 analysis of non-stationary signals. While correlation gives a static information about the
87 overall relationship between two variables, wavelet coherence normalises the cross wavelet
88 spectrum by their respective wavelet power spectra resulting in a coherence measure that
89 ranges from 0 (no correlation) to 1 (perfect correlation) along the time series for any
90 given period. Though comparison of spectra between periods within a narrow band is
91 permissible at higher periods, cross period comparison can't be made beyond a certain
92 ord due to emphasis of normalization on wavelet power at higher period (Maraun and
93 Kurths, 2004). This is where filtering techniques are applied to compare the strength of
94 variability across different frequency bands.

95 **S2.2.2 Filtering method**

96 Filtering is a signal processing method used to isolate variability within a specific fre-
97 quency band by suppressing signals outside that range. The Lanczos filter, commonly
98 used for this purpose, effectively reduces spectral leakage while preserving the signal of
99 interest (Duchon, 1979). A shortcoming of filtering method is loss of data at the begin-
100 ning and end of time series depending on the length of filtering window. While wavelet
101 analysis captures how variability evolves across all timescales, Lanczos filtering focuses
102 on fluctuations within a selected band, enabling direct comparisons between frequency
103 bands ([Tabletable S3, S4, Figs. S4–S9](#)). Note that the negative (positive) numbers in
104 filtered biomass is representing deviation i.e., decrease (increase) from the mean.

105 **S3 Quality control tests for Kollam (2020)**

106 The interannual variability appears particularly strong off Kollam, indicating uncertainty
107 about potential data quality issues. To investigate this, the following analyses were
108 conducted on the 2019–2020 biomass dataset from the Kollam: 1) assessment of pre-
109 deployment tests and base echo intensity (Er) prior to deployment in 20 October 2019,
110 2) comparison between in-situ MPN biomass and corresponding backscatter values post
111 deployment.

112 The first analysis assesses the sensitivity accuracy of the ADCP instrument (Fig. S10,
113 top panel). Given that the ADCP was retrieved and redeployed, its baseline echo intensity
114 is expected to remain stable across servicing. However, following its redeployment on
115 20 October 2019 off Kollam, the initial reference profile used to establish the base echo in-
116 tensity showed anomalously high values. This indicated an apparent drop in backscatter,
117 raising concerns regarding possible calibration, sensitivity, or deployment-related incon-
118 sistencies.

119 To further investigate, the second analysis examined in-situ biomass samples collected
120 post-deployment from the same region. These samples supported the backscatter observa-
121 tions: measured biomass was notably lower and deviated beyond one standard deviation
122 from the least-squares biomass–backscatter regression line. This alignment strengthens
123 the case for a real reduction in biomass rather than an instrumental error (Fig. S10,
124 bottom panel). At the same time, it underscores the importance of in-situ sampling in
125 validating long-term ADCP-derived observations. Without these direct measurements,
126 confidence in a year-long deployment would be limited. In this instance, low backscat-
127 ter coincides with genuinely low biomass, demonstrating the complementary value of
128 both approaches. The evaluation of backscatter and biomass before retrieval and af-
129 ter deployment highlights the critical role of in-situ biomass measurements in validating
130 backscatter-derived biomass estimates.

131 **S4 Caveats and strengths of ADCP backscatter as a 132 proxy for zooplankton biomass**

133 To investigate seasonal variability in zooplankton abundance in the Arabian Sea, the
134 JGOFS program conducted three cruises during distinct seasons: inter-monsoon (Apr–May
135 1994), winter (Feb–Mar 1995), and summer (Jul–Aug 1995), with sampling conducted
136 twice daily (midday and midnight) at each station (Madhupratap et al., 1996). However,
137 using just two temporal snapshots to represent an entire season may not adequately cap-
138 ture the dynamic nature of zooplankton biomass. The spatial map of mesozooplankton
139 distribution, such as the one by Jyothibabu et al. (2010) for each season (see Fig. 11
140 of Jyothibabu et al. (2010)) is limited by sampling frequency and time elapsed to cover
141 stations, and the measured biomass is prone to distortion.

142 Consider the summer monsoon months off Mumbai during early June of 2019 (Fig. 10),
143 where a spike in biomass is observed due to an instantaneous increase in the high-
144 frequency components of biomass variability, resulting in an increase of $\sim 150 \text{ mg m}^{-3}$
145 within a few days. Similar spikes are seen at other locations too, e.g., off Kollam during
146 the end of July and multiple instances in September of 2019. These spikes last only
147 for a day to a few days, but the bursts in biomass tend to last longer, from a few days
148 to a few weeks. This burst is also observed off Kollam, Udupi, and Goa, albeit with
149 decreasing intensity as we go poleward (Fig. 10, [Tabletable](#) S2). Such coherency can
150 only be observed if continuous and frequent measurements were taken across EAS. These
151 limitations highlight the need for high-resolution, continuous observations, such as those
152 provided by ADCP backscatter, to accurately assess zooplankton variability in time and
153 space.

154 **References**

- 155 P. Amol, D. Shankar, V. Fernando, A. Mukherjee, S. G. Aparna, R. Fernandes, G. S.
156 Michael, S. T. Khalap, N. P. Satelkar, Y. Agarvadekar, M. G. Gaonkar, A. P. Tari,
157 A. Kankonkar, and S.P. Vernekar. Observed intraseasonal and seasonal variability of
158 the West India Coastal Current on the continental slope. *J. Earth Syst. Sci.*, 123(5):
159 1045–1074, 2014. doi: 10.1007/s12040-014-0449-5.
- 160 S. G. Aparna, D. V Desai, D Shankar, A. C Anil, Shrikant Dora, and R. R. Khedekar.
161 Seasonal cycle of zooplankton standing stock inferred from ADCP backscatter mea-
162 surements in the eastern Arabian Sea. *Prog. Oceanogr.*, 203:102766, 2022. doi: 10.1016/
163 j.pocean.2022.102766.
- 164 Anya Chaudhuri, D. Shankar, S. G. Aparna, P. Amol, V. Fernando, A. Kankonkar, G. S.
165 Michael, N. P. Satelkar, S. T. Khalap, A. P. Tari, M. G. Gaonkar, S. Ghatkar, and R. R.
166 Khedekar. Observed variability of the West India Coastal Current on the continental
167 slope from 2009–2018. *J. Earth Syst. Sci.*, 129(1):57, 2020. doi: 10.1007/s12040-019-
168 1322-3.
- 169 Anya Chaudhuri, P Amol, D Shankar, S Mukhopadhyay, S. G Aparna, V Fernando,
170 and A Kankonkar. Observed variability of the West India Coastal Current on the
171 continental shelf from 2010–2017. *J. Earth Syst. Sci.*, 130:1–21, 2021. doi: 10.1007/
172 s12040-021-01603-4.
- 173 Claude E Duchon. Lanczos filtering in one and two dimensions. *J. Appl. Meteorol.*
174 *Climatol.*, 18(8):1016–1022, 1979. doi: 10.1175/1520-0450(1979)018<1016:LFIOAT>2.
175 0.CO;2.
- 176 Tommy G Jensen. Equatorial variability and resonance in a wind-driven Indian Ocean
177 model. *J. Geophys. Res. Oceans*, 98(C12):22533–22552, 1993. doi: 10.1029/93JC02565.
- 178 R Jyothibabu, N. V Madhu, H Habeebrehman, K. V Jayalakshmy, K. K. C Nair, and C. T
179 Achuthankutty. Re-evaluation of ‘paradox of mesozooplankton’ in the eastern Arabian
180 Sea based on ship and satellite observations. *J. Mar. Syst.*, 81(3):235–251, 2010. doi:
181 10.1016/j.jmarsys.2009.12.019.
- 182 M Madhupratap, T. C Gopalakrishnan, P Haridas, K. K. C Nair, P. N Aravindakshan,
183 G Padmavati, and Shiney Paul. Lack of seasonal and geographic variation in mesozoo-
184 plankton biomass in the Arabian Sea and its structure in the mixed layer. *Curr. Sci.*,
185 71(11):863–868, 1996. URL drs.nio.org/drs/handle/2264/2154.
- 186 Douglas Maraun and Jürgen Kurths. Cross wavelet analysis: significance testing and
187 pitfalls. *Nonlin. Processes Geophys.*, 11(4):505–514, 2004. doi: 10.5194/npg-11-505-2004.
- 188 Friedrich A. Schott and Julian P. McCrea. The monsoon circulation of the Indian
189 Ocean. *Prog. Oceanogr.*, 51(1):1–123, 2001. ISSN 0079-6611. doi: 10.1016/S0079-
190 6611(01)00083-0.
- 191 Christopher Torrence and Gilbert P Compo. A practical guide to wavelet analysis. *Bull.*
192 *Am. Meteorol. Soc.*, 79(1):61–78, 1998. doi: 10.1175/1520-0477(1998)079<0061:APGTWA>
193 2.0.CO;2.

Table S1:

The mean, standard deviation and range of ZSS (gm m^{-2}) and Chl-a (mg m^{-3}) *climatology* is presented for the seven locations. The SD gives information about the spread in values of each variable, while range indicates the difference between peak and trough of the same variable.

Mooring location	Chlorophyll			ZSS		
	Mean	SD	Range	Mean	SD	Range
Okha	0.51	0.24	0.72	20.5	1.8	5.8
Mumbai	0.33	0.13	0.39	23.6	2.6	8
Jaigarh	0.27	0.05	0.15	24.2	2.9	9
Goa	0.28	0.15	0.55	21.2	1.9	6.3
Udupi	0.59	0.56	1.54	21.9	1.9	5.8
Kollam	0.64	0.7	2.26	24.6	1.1	4.1
Kanyakumari	0.61	0.52	1.62	20.1	0.6	2.4

Table S2:

The mean, standard deviation at 40 and 104 m of zooplankton biomass (mg m^{-3}) at 7 mooring sites are tabulated based on the corresponding *daily data*. The last column represents the biomass range between the mean at 40 m and that at 104 m.

Mooring location	40 m biomass		104 m biomass		Decrease with depth (40 m - 104 m)
	Mean	SD	Mean	SD	
Okha	212.8	27.5	143.6	29.7	69.2
Mumbai	248.6	37.2	169.8	34.6	78.8
Jaigarh	253.5	38.2	170.4	50	83.1
Goa	216.3	35	153.5	37.2	62.8
Udupi	227.6	39.7	158.8	38.4	68.8
Kollam	247.9	55.5	184.2	48.3	63.7
Kanyakumari	192.3	34.4	157.5	23.8	34.8

Table S3:

SD of all distinct variability components of 40 m biomass each location with 104 m biomass variability shown in brackets, the units are in mg m^{-3} . The first column shows variance of seasonal cycle, a combination of variability in annual and intra-annual band. Note that the intraseasonal variability (5–90 days) band is comparable and on few locations stronger than the seasonal variability, indicating higher fluctuations occurring within a season.

Mooring location	Seasonal (100-400 days)	Annual (300-400 days)	Intra-annual (100-250 days)	Intraseasonal (5-90 days)
Okha	6.3 (14.2)	2.3 (2.5)	4.9 (10.1)	17.7 (16.7)
Mumbai	19.1 (19.4)	5.6 (5.8)	13.2 (12.7)	20.2 (19.8)
Jaigarh	14.4 (20.9)	5.4 (7.9)	12.1 (12)	21.1 (23.8)
Goa	16.2 (17.8)	2.9 (6.5)	12.3 (10.1)	20.2 (17)
Udupi	22.1 (25)	4.9 (8.3)	15.2 (15.1)	23.7 (15.5)
Kollam	24.3 (15.6)	6.5 (5.1)	18.4 (10.9)	26.7 (17.4)
Kanyakumari	14.1 (9)	3.8 (3.4)	10 (5.6)	21.2 (14.3)

Table S4:

SD of all distinct components of ZSS (chl-*a*) variability using it's daily data, the units are in mg m^{-2} (mg m^{-3}). The first column shows variance of seasonal cycle, a combination of variability in annual and intra-annual band. The chl-*a* for Mumbai and Jaigarh lacks valid values except for intraseasonal band owing to data gaps.

Mooring location	Seasonal (100-400 days)	Annual (300-400 days)	Intra-annual (100-250 days)	Intraseasonal (5-90 days)
Okha	0.7 (0.3)	0.2 (0.1)	0.5 (0.2)	1.1 (0.4)
Mumbai	1.6 (-)	0.5 (-)	0.9 (-)	1.2 (0.1)
Jaigarh	1.9 (-)	0.7 (-)	0.9 (-)	1.4 (0.1)
Goa	1.5 (0.1)	0.4 (0)	1 (0.1)	1.1 (0.1)
Udupi	1.8 (0.5)	0.3 (0.1)	1.3 (0.3)	1.2 (0.7)
Kollam	1 (0.6)	0.1 (0.2)	0.9 (0.5)	1.5 (0.7)
Kanyakumari	0.7 (0.5)	0.2 (0.1)	0.5 (0.3)	1.3 (0.7)

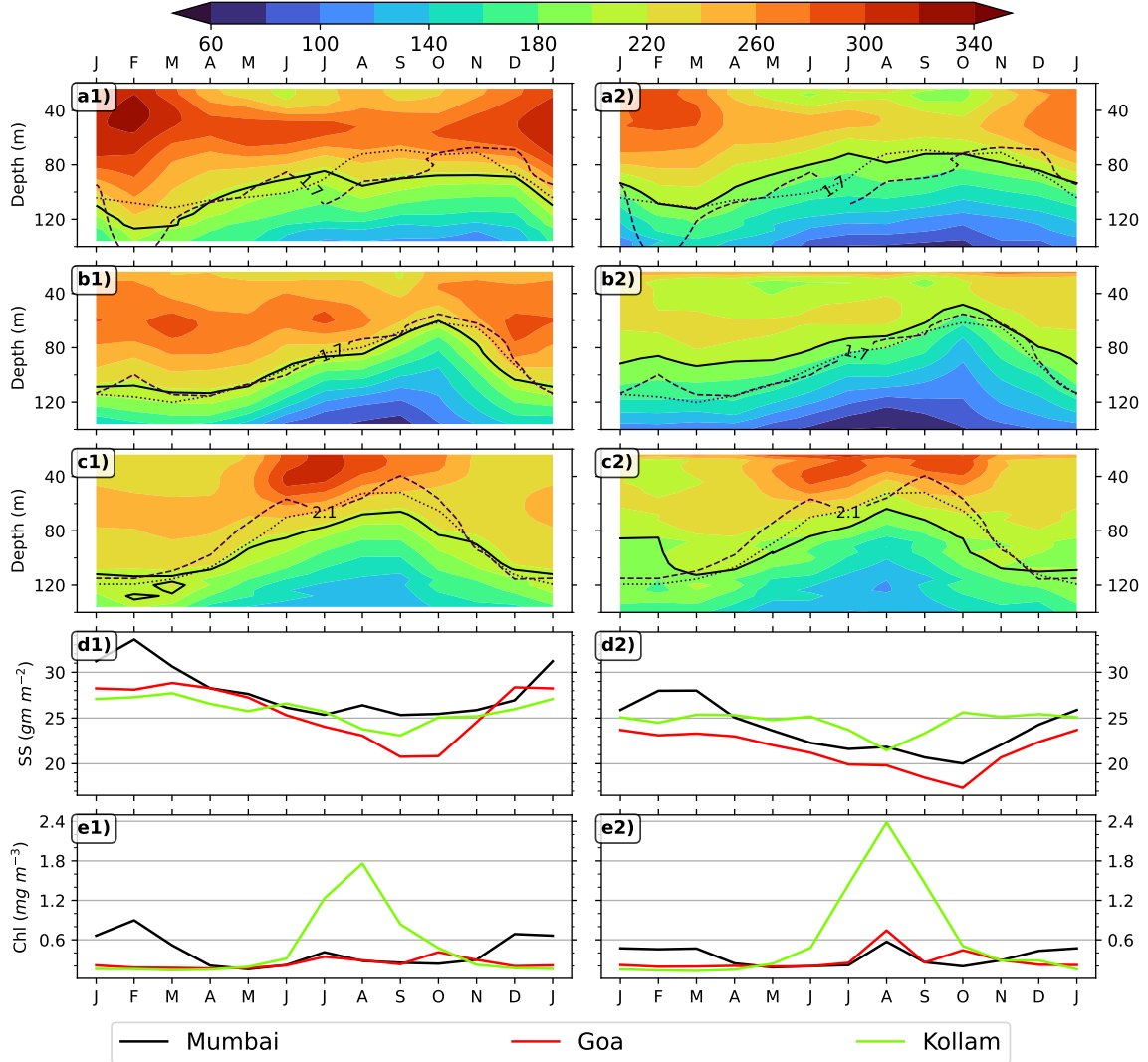


Figure S1: Monthly climatology of zooplankton biomass is shown in left panels for 3 locations which were earlier used in (Aparna et al., 2022); a1, b1 & c1 is the biomass climatology for Mumbai, Goa and Kollam, d1 is for ZSS climatology (24–140 biomass integral), e1 is for chl-a biomass climatology; a2, b2, c2, d2 & e2 is same but based on data from 2017 to 2023. The D215 is shown in solid black. The dashed line represents the depth of 23 °C isotherm; oxygen contours are shown in dotted lines and labeled for each location.

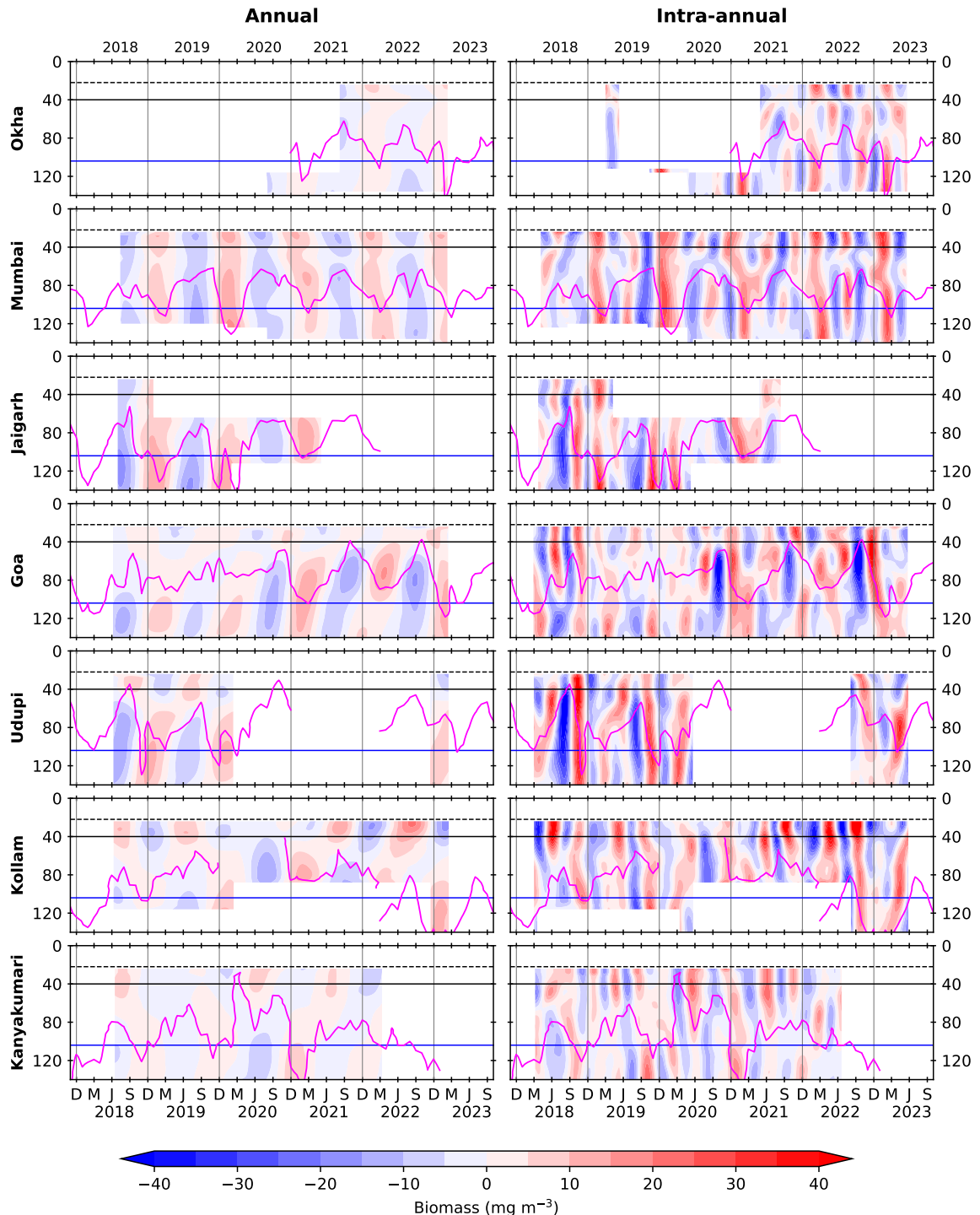


Figure S2: The biomass variation occurring in annual band (300 to 400 days) and intra-annual band (100 to 250 days) is obtained using a band pass filter. The horizontal black and blue lines is for 40 and 104 m, vertical black lines separate the years. Dashed line at 22 m marks the top-depth of first bin i.e, 24 m and solid magenta curves denotes D215 (D175 off Okha and Kanyakumari) obtained from monthly biomass time series.

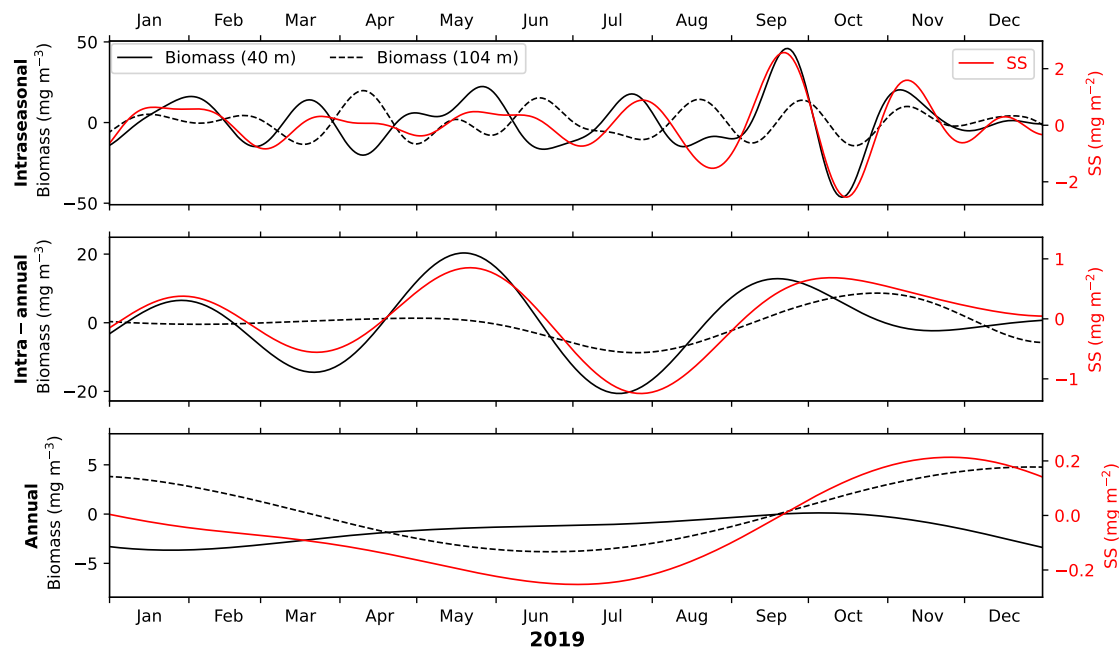


Figure S3: The 40 and 104 m biomass in comparison with ZSS (column integrated standing stock). The biomass at 104 m may or may not be in phase with upper ocean biomass at 40 m, thereby enhancing or diminishing ZSS variation and it is seen at all the distinct bands of variability.

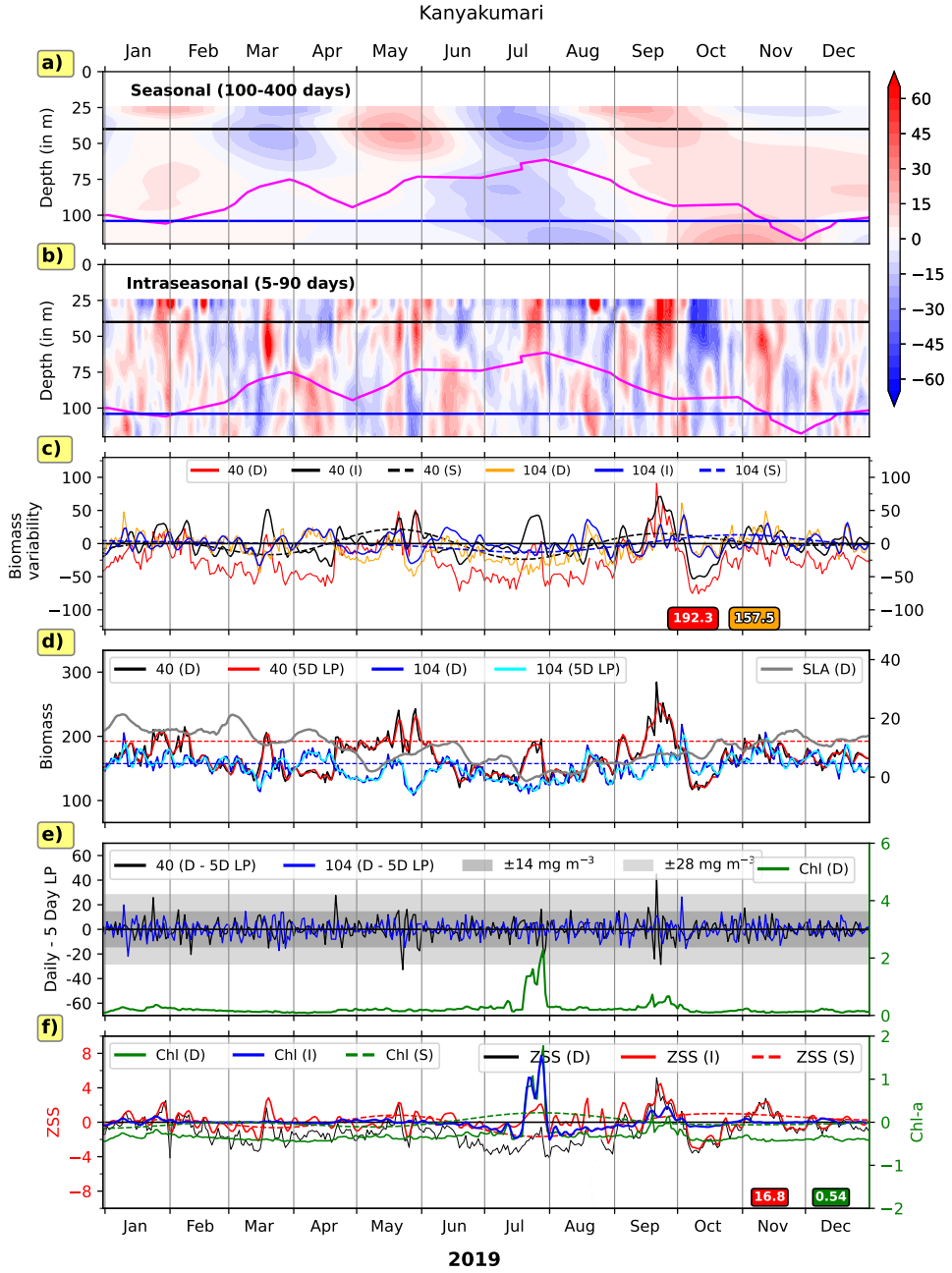


Figure S4: Panel of plots showing comparison of variability in seasonal and intraseasonal band off Kanyakumari. The first two panel shows time vs depth plot of seasonal and intraseasonal biomass in same scale: 40 (104) m depths are marked by black (blue) lines, and vertical Grey line separate months, magenta curve shows D175. The third panel from top shows 40 and 104 m daily, intraseasonal (5–90 days), and seasonal (100- 400 days) biomass, mean of daily biomass for respective depth is shown in bottom right of the panel. The fourth panel represents the daily biomass overlaid by 5 day low-pass filtered biomass and daily SLA. Notice the high (low) SLA coinciding with lower (higher) 40 m biomass. The fifth panel shows the difference between daily and 5 day low-pass filtered biomass at 40 and 104 m, Grey (light Grey) shaded region highlights SD (2SD) region of backscatter-biomass equation onto which the daily Chl-*a* is overlaid. The bottom-most panel shows the Chl-*a* and ZSS in Intraseasonal and seasonal band.

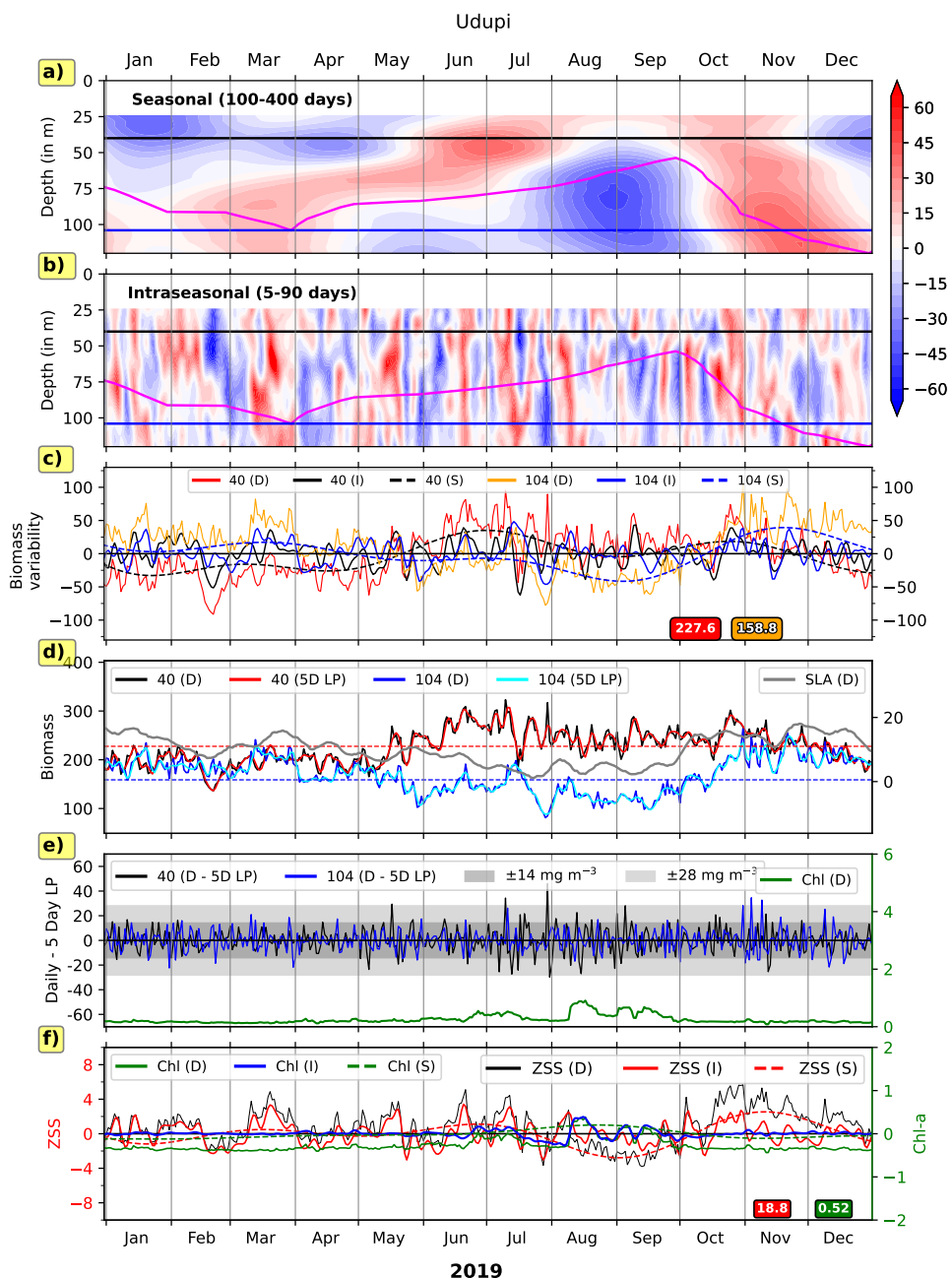


Figure S5: Same as in Fig. S4 but for Udupi with D215 curve in top two panels.

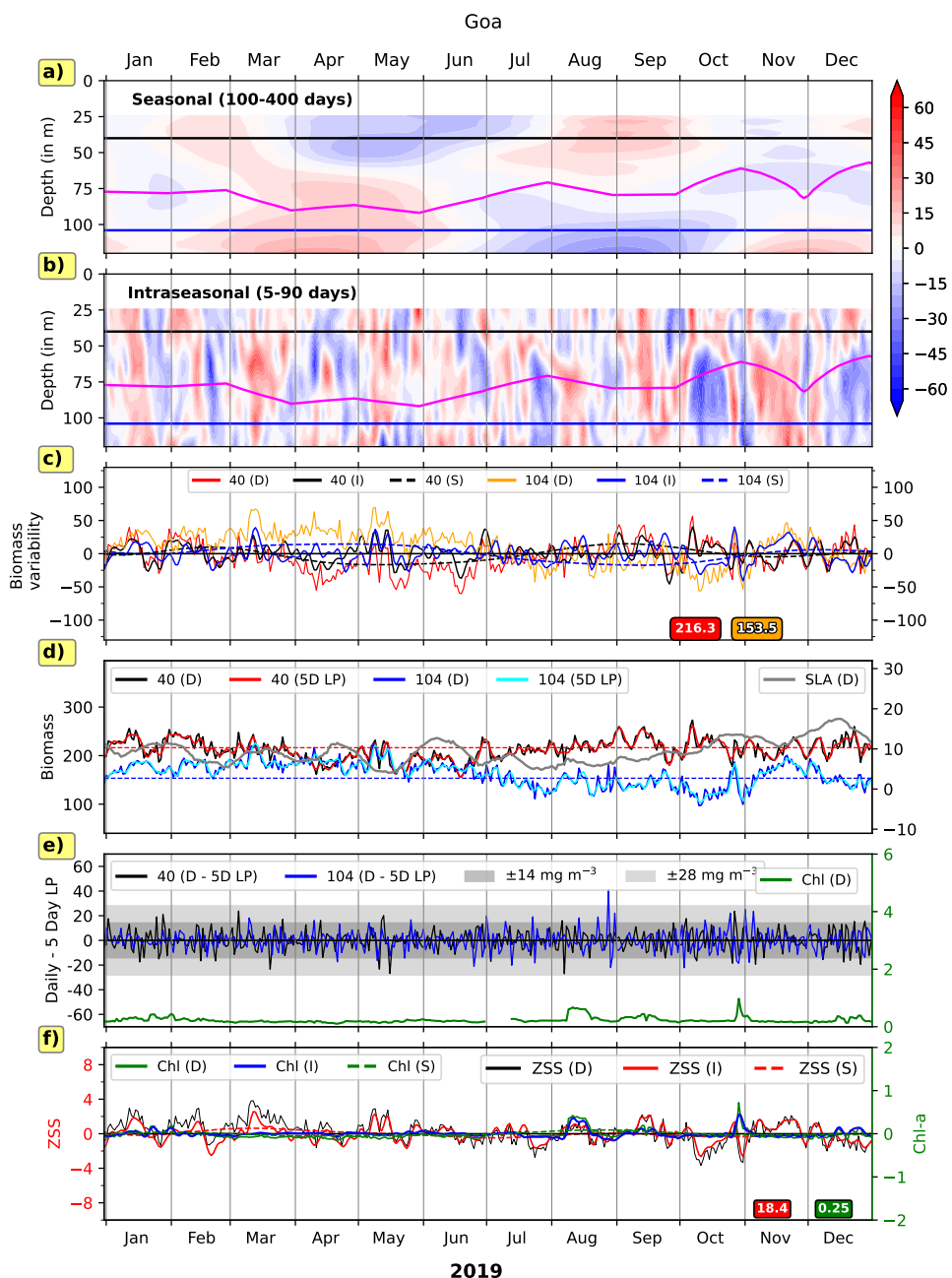


Figure S6: Same as in Fig. S4 but for Goa with D215 curve in top two panels.

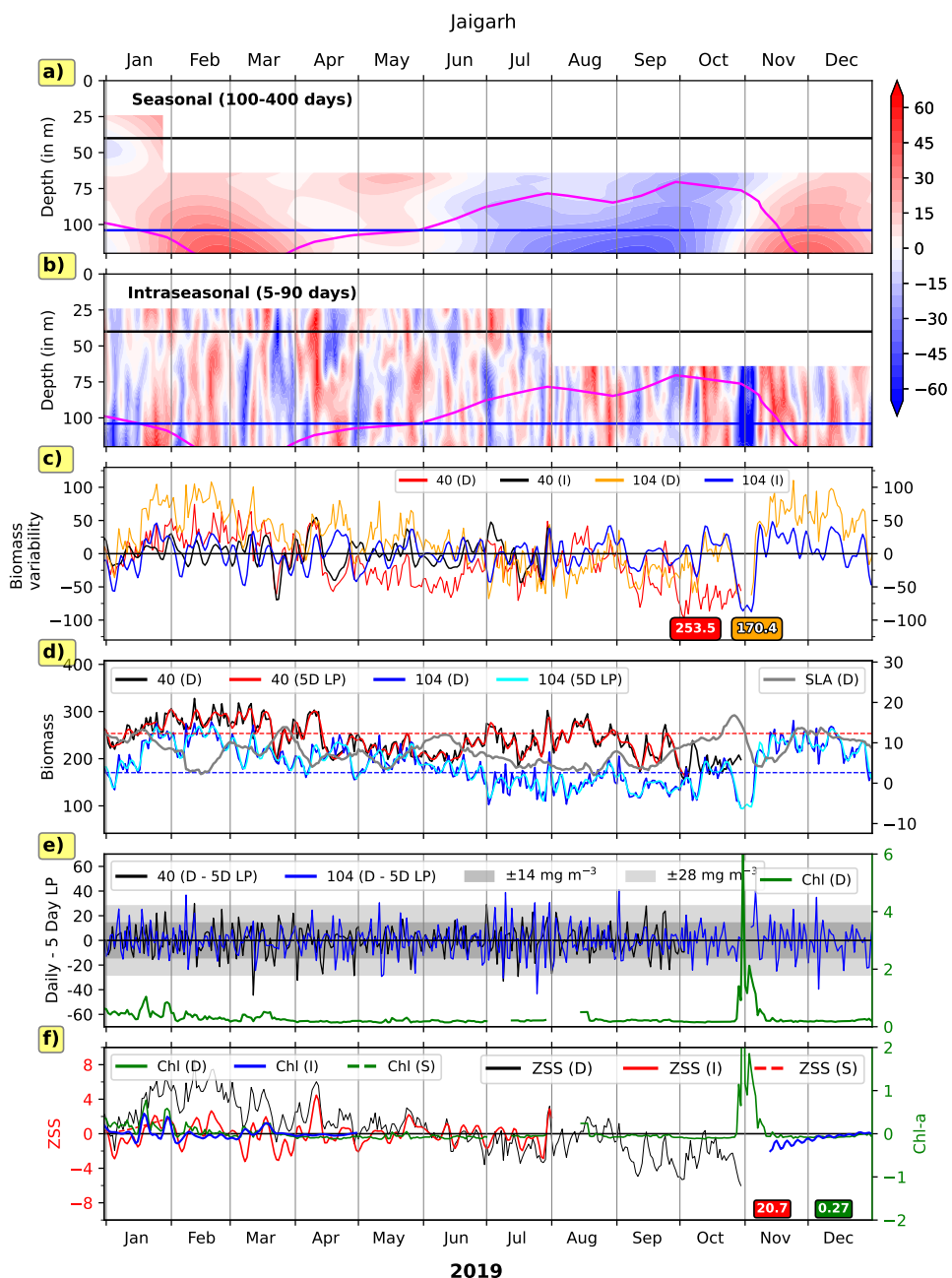


Figure S7: Same as in Fig. S4 but for Jaigarh with D215 curve in top two panels.

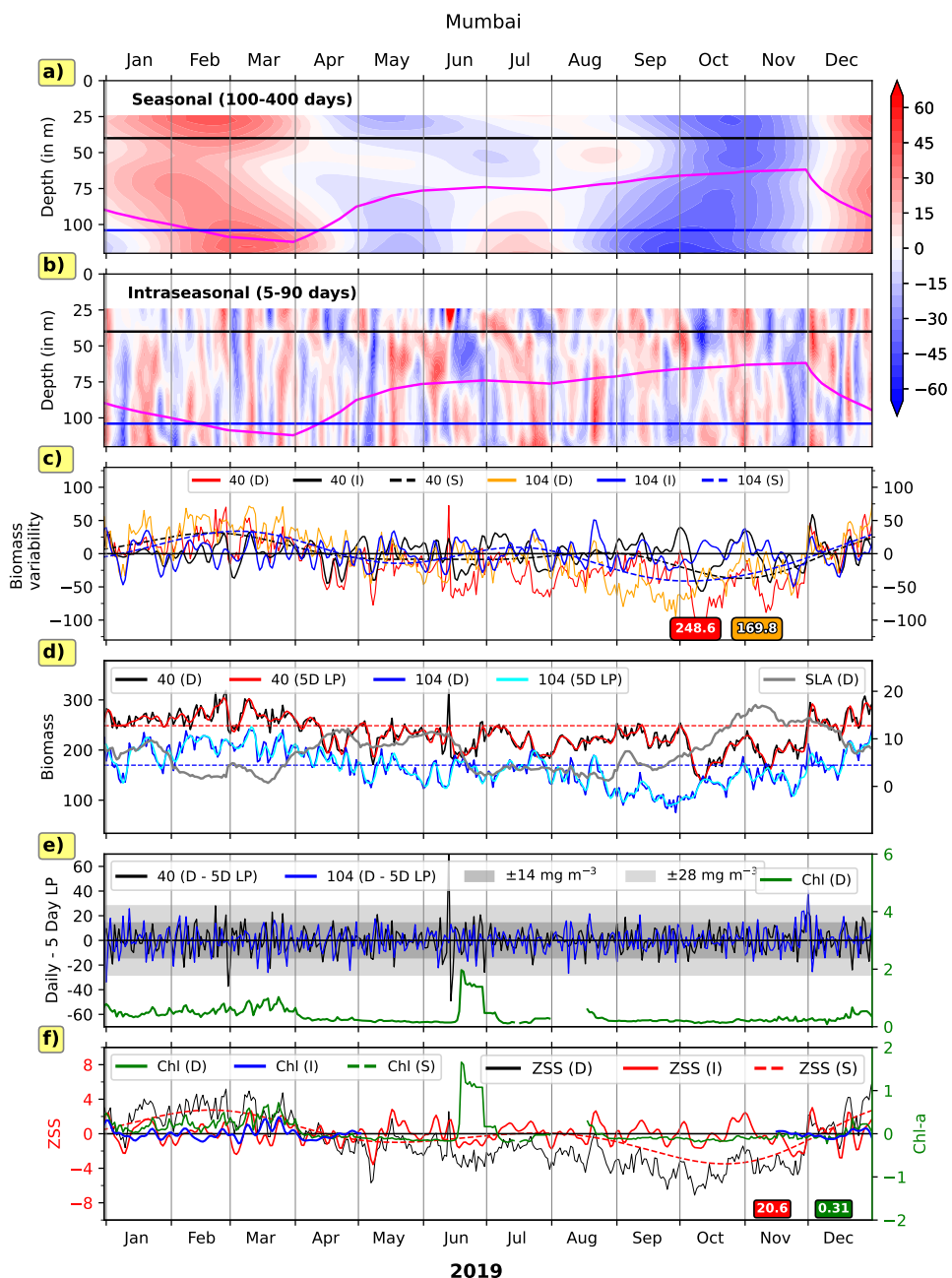


Figure S8: Same as in Fig. S4 but for Mumbai with D215 curve in top two panels.

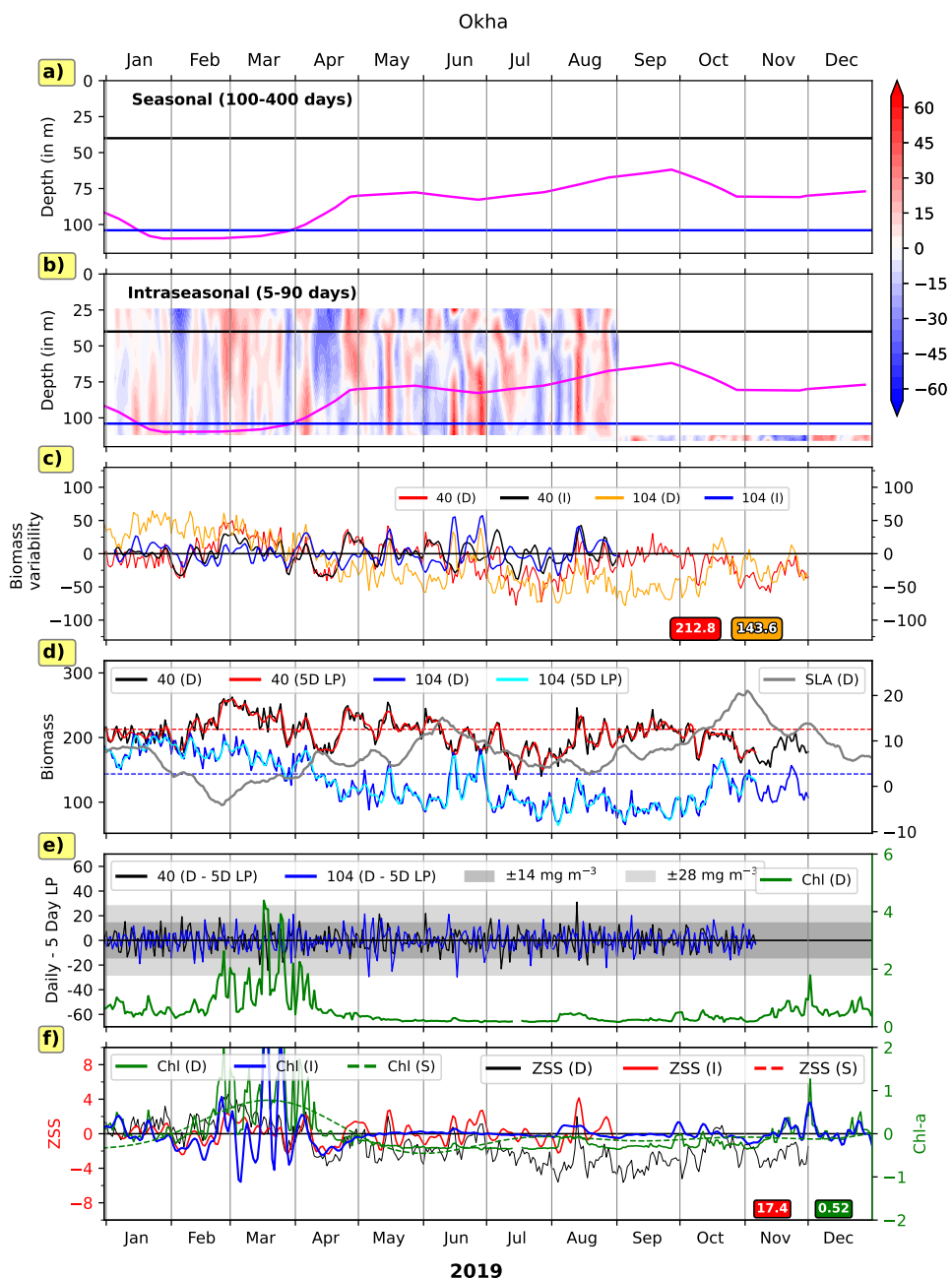


Figure S9: Same as in Fig. S4 but for Okha with D175 curve in top two panels.

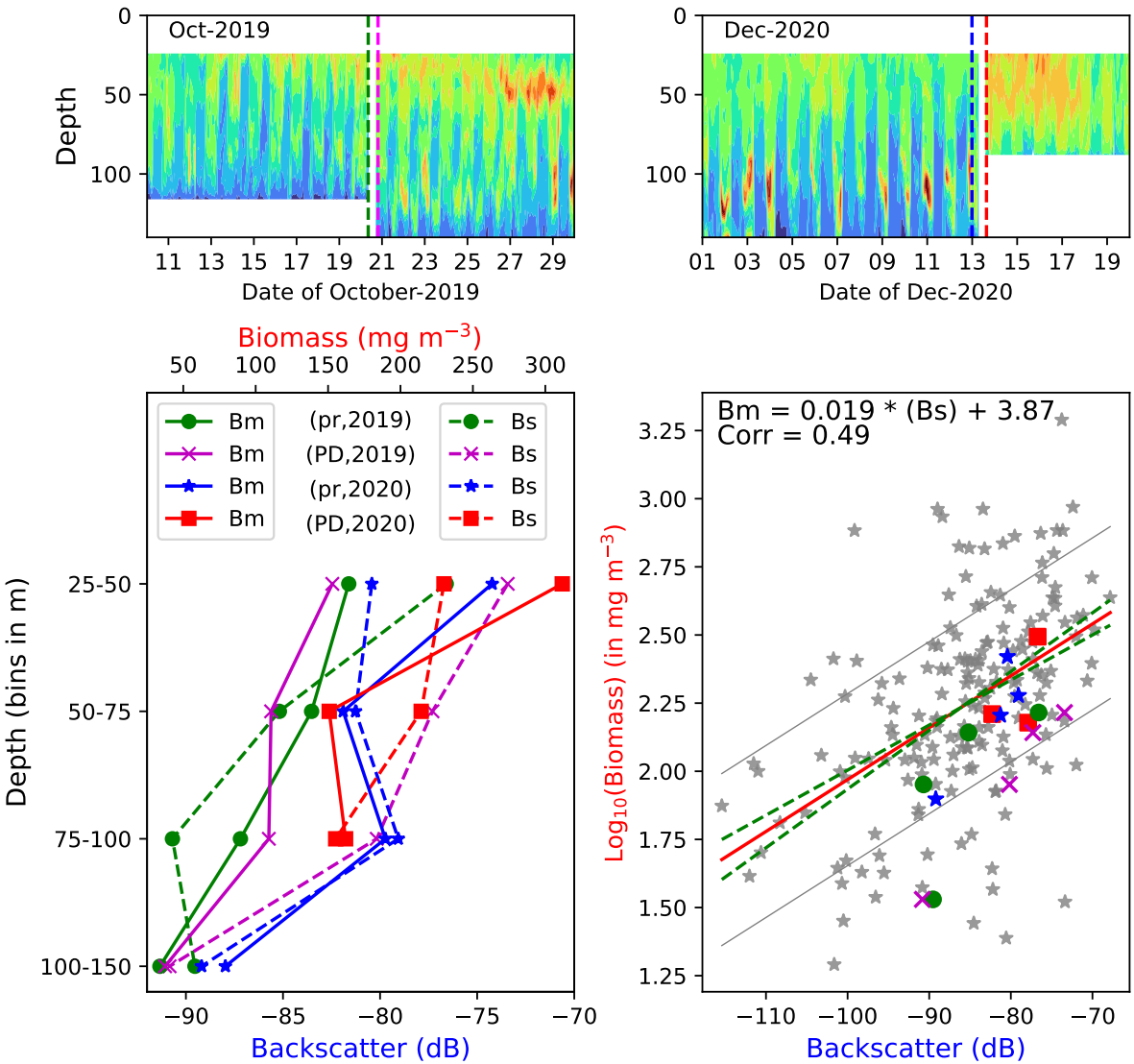


Figure S10: The 40-and-104-m top panel shows the hourly biomass in comparison off Kollam, with ZSS the retrieval (column-integrated standing stock dashed black line) and deployment (dashed magenta line) events marked in October 2019 and December 2020, respectively. The bottom left panel presents in-situ biomass at 104 m may or may not be in phase with upper ocean profiles (Bm) as solid lines and corresponding backscatter profiles (Bs) as dashed lines for the pre-retrieval (PR) and post-deployment (PD) phases of 2019 and 2020. The bottom right panel displays biomass at 40 m, thereby enhancing or diminishing ZSS variation (log₁₀ scale) plotted against backscatter for Kollam in 2019 and it is seen at 2020, overlaid on the linear regression line fitted to all available data points. Symbols used in this panel match those in the distinct bands of variability bottom left panel.

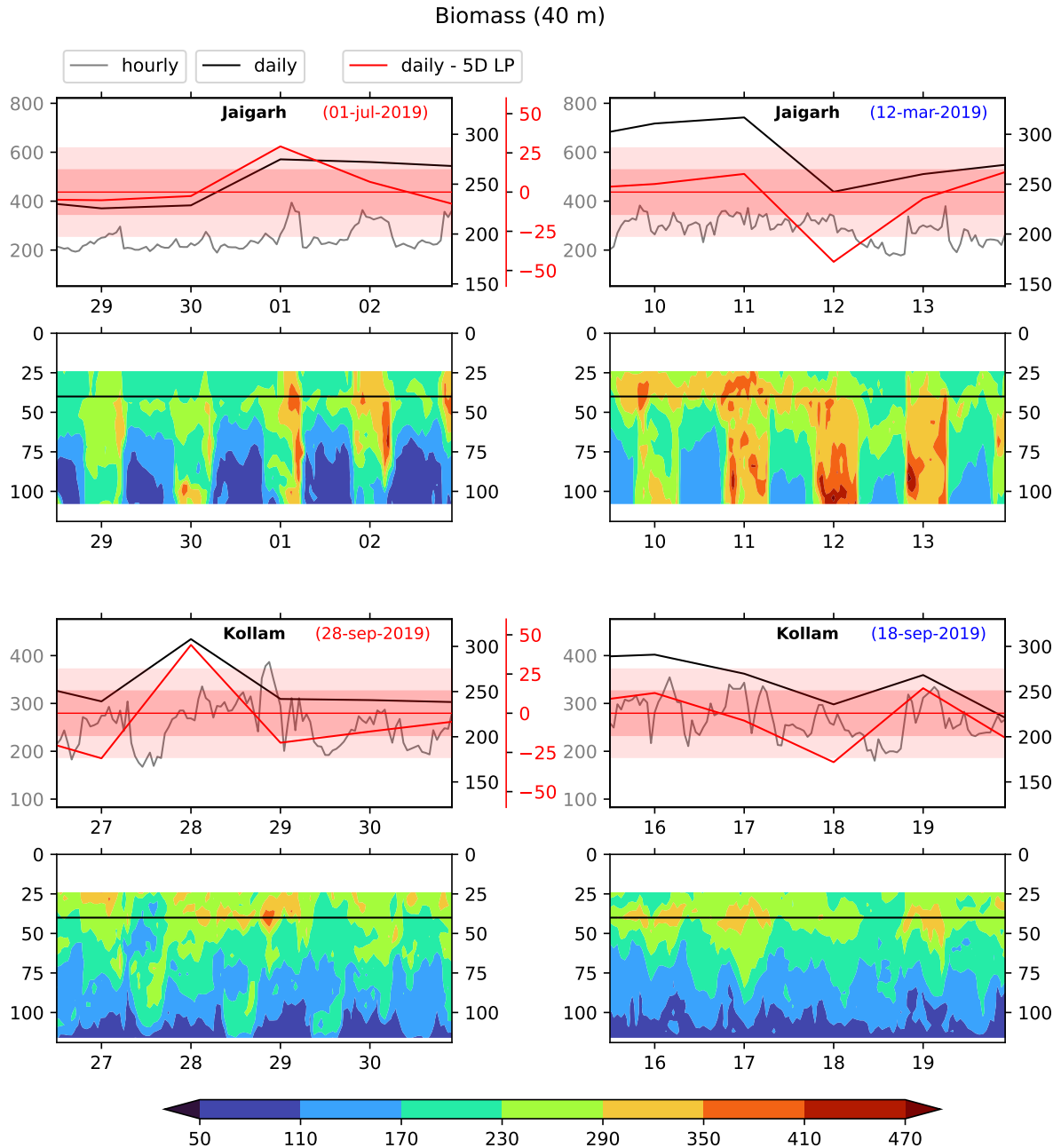


Figure S11: Spikes are shown as the difference between the mean-removed daily biomass time series (red line) and the 5-day low-pass filtered biomass (black line) at 40 m depth, off Jaigarh and Kollam. The overlaid hourly time series illustrates the actual biomass variation throughout the day. Shaded regions represent ± 1 SD(red) and ± 2 SD (light red) from the mean-removed daily time series. The date of spike occurrence is noted in the top-right corner of each panel, with red and blue text indicating positive and negative spikes, respectively.

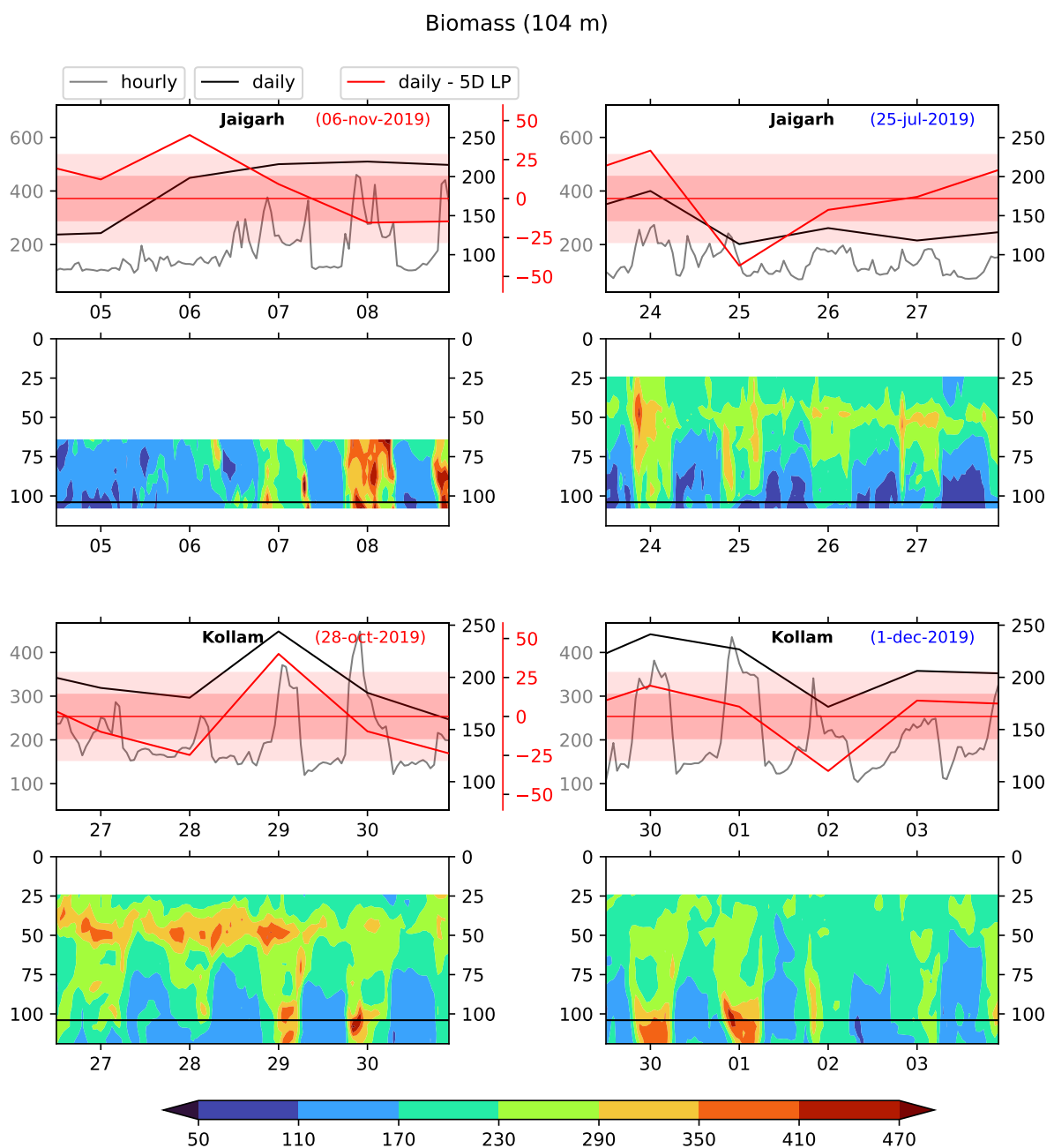


Figure S12: Same as Fig. S11 but for biomass at 104 m depth.